

Galaxy clusters and structure formation in quintessence versus phantom dark energy Universe

Zacharias Roupas,^{1,*} Minos Axenides,^{1,†} George Georgiou,^{1,‡} and Emmanuel N. Saridakis^{2,3,§}

¹*Institute of Nuclear and Particle Physics, N.C.S.R. Demokritos, GR-15310 Athens, Greece*

²*Physics Division, National Technical University of Athens, 15780 Zografou Campus, Athens, Greece*

³*Instituto de Física, Pontificia Universidad Católica de Valparaíso, Casilla 4950, Valparaíso, Chile*

The self-gravitating gas in the Newtonian limit is studied in the presence of dark energy with a linear equation of state. Entropy extremization associates to the isothermal Boltzmann distribution an effective density that includes ‘dark energy particles’, which either strengthen or weaken mutual gravitational attraction, in case of quintessence or phantom dark energy, respectively. Stability is studied for microcanonical (fixed energy) and canonical (fixed temperature) ensembles. Compared to the previously studied cosmological constant case, in the present work it is found that quintessence increases, while phantom dark energy decreases the instability domain under gravitational collapse. Thus, structures are more easily formed in a quintessence rather than in a phantom dominated Universe. Assuming that galaxy clusters are spherical, nearly isothermal and in hydrostatic equilibrium we find that dark energy of any kind, for fixed radius, mass and temperature, steepens their total density profile! In case of a cosmological constant, this effect accounts for a 1.5% increase in the density contrast, that is the center to edge density ratio of the cluster. We also propose a method to constrain phantom dark energy.

I. INTRODUCTION

Dark energy is considered a main component of our universe, since its existence relies on convincing observational data [1–3]. However, its nature still remains a mystery for physics. Three main candidates are quintessence [4–10], the cosmological constant and phantom dark energy [11–16].

In this expanding universe, driven by dark energy, structures form by the gravitational instability of the self-gravitating gas, that causes a density perturbation to decouple from expansion and collapse. In the matter dominated era, the velocity of gas’ constituents is low and the Newtonian limit is appropriate. The thermodynamic stability of a self-gravitating gas in the Newtonian limit is a very old subject [17–24] (the relativistic case has recently earned a lot of attention [25–32]). Hence, this subject has not only a pure theoretical interest, but also an additional cosmological motivation. Its direct application to large structures in the universe, such as the galaxy clusters, provides information on their formation and evolution. Furthermore, one can extend [33, 34] this analysis and investigate the effects of a cosmological constant on the stability of the self-gravitating gas [35–37].

In the present work we extend these latter studies [35–37] in order to examine the effects of a general dark energy sector on the stability of isothermal spheres and galaxy clusters. In particular, we would like to see how the galaxy clusters and especially their more massive component, namely the dark matter haloes, are affected

by the presence of a quintessence or a phantom dark energy, parametrized by a linear equation of state. As we will see, compared to the simple cosmological constant Λ case, apart from increasing the repulsion due to the negative pressure, phantom dark energy in the Newtonian description introduces effective “dark energy particles” that weaken gravitational attraction. On the other hand, quintessence has the inverse effects, that is it decreases repulsion due to pressure and introduces dark energy particles that strengthen mutual gravitational attraction compared to the Λ case. Thus, for both reasons, phantom dark energy decreases the (under gravitational collapse) instability domain and quintessential dark energy increases the instability domain with respect to the Λ case. Large-scale structures are more difficult to be formed in a phantom universe rather than in a quintessence one. This is one main result of our analysis.

The potential effect of a dark-energy component on the formation of galaxy clusters has been inspected recently (see [38, 39] and References therein). As we will see, the dark-energy sector does indeed have effects on the density profile of galaxy clusters and mainly their most massive component, the dark matter haloes. We find that the effects are in principle detectable, and more interestingly that the density profile steepens, in contrast with naive expectation. Additionally, one can use these results the other way around, and impose constraints on the dark-energy equation-of state from galaxy-clusters observations.

The paper is organized as follows. In section II we present the thermodynamics of self-gravitating gas in the presence of dark energy and we study its effect on stability, studying hydrostatic equilibrium, calculating the entropy extrema and performing the stability analysis. In section III we study the galaxy clusters, investigating the effect of dark energy on the clusters’ density profile and proposing a method to constrain the dark energy

*Electronic address: roupas@inp.demokritos.gr

†Electronic address: axenides@inp.demokritos.gr

‡Electronic address: georgiou@inp.demokritos.gr

§Electronic address: Emmanuel.Saridakis@baylor.edu

equation of state, based on clusters observations. Finally, section IV is devoted to the conclusions.

II. THERMODYNAMIC INSTABILITIES AND DARK ENERGY

In order to investigate the dark energy effects on the stability of a self-gravitating gas, we will be based on our previous studies [35–37]. We assume that the dark energy sector is described by a perfect fluid of energy density ρ_X and pressure p_X , while its equation-of-state parameter is defined as

$$w \equiv \frac{p_X}{c^2 \rho_X}, \quad (1)$$

where for clarity we keep the light speed c in the equations. In the following we restrict ourselves to the observationally favored case $w < -\frac{1}{3}$, although this is not necessary. In this work we assume that $w = \text{const}$, as we want to consider the simplest possible setup, in order to understand the basic effects of dark energy. The extension to the full time-varying w and/or time-varying cosmological constant [40–42], as long as the incorporation of possible dark-energy dark-matter interactions [16, 43–45] and the corresponding complicated analysis, will follow in a subsequent work.

Let us now derive the modified Poisson equation with a dark energy component in the Newtonian limit. Denoting by ρ and p the gas' energy density and pressure, respectively, we can write down the total energy-momentum tensor as

$$T_\nu^\mu = [(p + p_X) + (\rho + \rho_X)c^2] g_{\alpha\nu} \frac{dx^\mu}{ds} \frac{dx^\alpha}{ds} - (p + p_X) \delta_\nu^\mu, \quad (2)$$

where $g_{\alpha\nu}$ is the spacetime metric with sign $[+, -, -, -]$, x^μ the spacetime coordinate of one fluid element and s

the proper length. In the non-relativistic limit, and assuming equilibrium (that is $d\vec{x}/ds = 0$) it becomes:

$$T_\nu^\mu \simeq [\rho + (1 + w)\rho_X] c^2 \delta_0^\mu \delta_\nu^0 - w \rho_X c^2 \delta_\nu^\mu. \quad (3)$$

Defining the gravitational potential ϕ as usual through

$$\frac{d^2 \vec{x}}{dt^2} = -\vec{\nabla} \phi,$$

we can calculate that for slowly moving particles $\Gamma_{00}^i \approx d^2 x^i / (c^2 dt^2) = \partial^i \phi / c^2$, and thus that in the static weak field (Newtonian) limit we have $R_0^0 = \frac{1}{c^2} \nabla^2 \phi$. Inserting these Newtonian-limit expressions in the time-time component of the Einstein's equations

$$R_\nu^\mu = \frac{8\pi G}{c^4} T_\nu^\mu - \frac{4\pi G}{c^4} T \delta_\nu^\mu, \quad (4)$$

we finally obtain

$$\nabla^2 \phi(r) = 4\pi G \rho + 4\pi G(1 + 3w)\rho_X. \quad (5)$$

This is the modified Poisson equation that determines the gravitational potential in the Newtonian limit.

A. Hydrostatic equilibrium

It will be instructive to study the hydrostatic equilibrium of the self-gravitating gas in presence of dark energy. We start with the relativistic equation of hydrostatic equilibrium, known as Tolman-Oppenheimer-Volkof (TOV) equation [46, 47], which however we need to derive in the presence of the dark energy component. As we show in detail in Appendix A, in the static, spherically symmetric case, the Einstein's equations reduce to two equations, namely

$$\frac{dp}{dr} = - \left[\frac{p}{c^2} + \rho + (1 + w)\rho_X \right] \left[\frac{G\mathcal{M}(r)}{r^2} + 4\pi G \frac{p}{c^2} r + \frac{4\pi G}{3} \rho_X r(1 + 3w) \right] \left(1 - \frac{2G\mathcal{M}(r)}{rc^2} - \frac{8\pi G}{3c^2} \rho_X r^2 \right)^{-1} \quad (6)$$

$$\frac{d\mathcal{M}(r)}{dr} = 4\pi \rho r^2, \quad (7)$$

where $\rho(r)$ and $p(r)$ are respectively the total mass-energy density and pressure at point r , and $\mathcal{M}(r)$ the total mass-energy contained inside r . The first equation (6) is the TOV equation in the presence of a dark-energy component. In the Newtonian limit, that is for $c \rightarrow \infty$, we obtain

$$\frac{dp}{dr} = - [\rho + (1 + w)\rho_X] \left[G \frac{\mathcal{M}(r)}{r^2} + \frac{4\pi G}{3} \rho_X r(1 + 3w) \right], \quad (8)$$

where ρ now is the density of matter. This is the equation of hydrostatic equilibrium in the presence of dark energy in the Newtonian limit.

We observe, that gravity is now exerted on effective matter with density

$$\rho_{\text{eff}} = \rho + (1 + w)\rho_X. \quad (9)$$

This definition for the effective matter density is also inferred by the momentum component of the energy-

momentum tensor in the Newtonian limit, namely

$$T^{0i} = [\rho + (1+w)\rho_X] \frac{dx^i}{dt}, \quad (10)$$

as it straightforwardly arises from (2).

Note that looking at the Poisson equation (5), a naive guess would be to define the effective density as $\rho + (1+3w)\rho_X$ instead of (9). This would be wrong. Dark energy introduces an attractive part coming from ρ_X and a repulsive one coming from the negative pressure with three components. In case of a cosmological constant ($w = -1$) the attractive part is completely counterbalanced by the one pressure component, as is evident by the momentum (10), leaving only a term $-2\rho_X$ in the Poisson equation, without the need of introducing any kind of new matter. However, we see that in the general dark-energy case, apart from the repulsive gravity due to the pressure, in the Newtonian limit we have the effective appearance of additional ‘‘matter particles’’ that gravitate normally in the quintessence case ($\rho_{\text{eff}} > \rho$) or that tend to gravitationally neutralize normal matter in the phantom case ($\rho_{\text{eff}} < \rho$).

Let us determine the density distribution for which the equation of hydrostatic equilibrium (8) leads to the modified Poisson equation (5). For an isothermal distribution $T = \text{const.}$, the velocity distribution of the gas particles should be a Maxwellian:

$$f(r, v) = \left(\frac{m}{2\pi kT} \right)^{\frac{3}{2}} \frac{\rho_{\text{eff}}(r)}{m} e^{-\frac{m}{2kT} v^2/2}, \quad (11)$$

with m their masses, v their velocities, and k the Boltzmann constant. Respectively, the pressure writes as

$$p(r) \equiv \int f \frac{1}{3} m v^2 d^3v = \rho_{\text{eff}}(r) \frac{kT}{m}. \quad (12)$$

Thus, in order to get (5) from (8) we should have

$$\rho_{\text{eff}} = \rho_{0,\text{eff}} e^{-\frac{m}{kT} [\phi - \phi(0)]}, \quad (13)$$

which is just the Boltzmann distribution for ρ_{eff} . Inserting this to (9) we acquire

$$\rho = [\rho_0 + (1+w)\rho_X] e^{-\frac{m}{kT} [\phi - \phi(0)]} - (1+w)\rho_X. \quad (14)$$

Finally, substituting expressions (12), (13) and (14) into equation of hydrostatic equilibrium (8), we finally obtain

$$\frac{1}{r^2} \frac{d}{dr} \left(r^2 \frac{d\phi}{dr} \right) = 4\pi G \rho + 4\pi G \rho_X (1+3w), \quad (15)$$

that is the spherically symmetric version of the Poisson equation (5).

The fact that the effective density as defined in (9) does obey Boltzmann distribution, reassures us that it is the correct choice. We stress that the correct definition of the effective matter density is crucial, since it affects the calculation of the potential energy, but most importantly because it is the one measured in indirect mass observations (for instance in gravitational lensing measurements).

B. Entropy extremum

Let us prove that the distributions (11), (13) extremize the entropy and thus, that they describe thermodynamic equilibria. Let the self-gravitating gas be bounded by spherical walls. This condition is needed for the entropy to have an extremum. Equivalently, only under this condition can hydrostatic equilibrium exist for finite mass. Such a configuration is called an ‘‘isothermal sphere’’ [18, 48].

Let an isothermal sphere have radius R , and let

$$S = -k \int f(\vec{r}, \vec{v}) \log f(\vec{r}, \vec{v}) d^3\vec{r} d^3\vec{v}, \quad (16)$$

be the Boltzmann entropy, where the distribution $f(\vec{r}, \vec{v})$ provides the number of effective particles that are inside the cube $d^3\vec{r}$ at \vec{r} , with velocities from \vec{v} to $\vec{v} + d\vec{v}$. Thus, we have

$$\rho_{\text{eff}}(\vec{r}) = m \int f(\vec{r}, \vec{v}) d^3v, \quad (17)$$

and the total effective mass is

$$M_{\text{eff}} = m \int f d^6\tau, \quad (18)$$

with $d^6\tau = d^3\vec{r} d^3\vec{v}$. In order to calculate the distribution f that extremizes the entropy S , we have to calculate the variation of (16) in terms of f .

The Poisson equation (5) can be written as

$$\nabla^2 \phi(r) = 4\pi G \rho_{\text{eff}} + 8\pi G w \rho_X. \quad (19)$$

We see that the effective particles interact mutually with Newtonian gravity and moreover interact with some repulsive potential. Hence, we can define the effective potentials

$$\phi_{N(\text{eff})} = -G \int \frac{\rho_{\text{eff}}(\vec{r}')}{|\vec{r} - \vec{r}'|} d^3\vec{r}' \quad (20)$$

$$\phi_{X(\text{eff})} = \frac{4\pi G}{3} w \rho_X r^2, \quad (21)$$

with the total potential being

$$\phi = \phi_{N(\text{eff})} + \phi_{X(\text{eff})} \quad (22)$$

and therefore the total potential energy takes the simple form

$$U = \frac{1}{2} \int \rho_{\text{eff}} \phi_{N(\text{eff})} d^3\vec{r} + \int \rho_{\text{eff}} \phi_{X(\text{eff})} d^3\vec{r}. \quad (23)$$

Inserting (17) and (20) into (23), we straightforwardly find

$$U = -\frac{G}{2} \iint m^2 f(\vec{r}, \vec{v}) \frac{f(\vec{r}', \vec{v}')}{|\vec{r} - \vec{r}'|} d^6\tau' d^6\tau + \int m f \phi_{X(\text{eff})} d^6\tau. \quad (24)$$

We want to extremize the entropy with constant energy and mass. Using the Lagrange's multipliers method, the following variation condition should be satisfied to first order:

$$\delta S/k - \beta \delta E + \alpha \delta M_{\text{eff}} = 0, \quad (25)$$

where β , α are two yet undetermined Lagrange multipliers and k the Boltzmann's constant. Inserting δS from (16) and δM_{eff} from (18), as well as calculating from (24) that $\delta E = m \int \delta f (v^2/2 + \phi - C) d^6\tau$, with $C = 2\pi G(1+w)\rho_X R^2$, we finally acquire from (25) that:

$$\log f + 1 + m\beta \left(\frac{v^2}{2} + \phi - C \right) - m\alpha = 0. \quad (26)$$

This finally gives

$$f(r, v) = A e^{-\beta m [\frac{1}{2}v^2 + \phi(r)]}, \quad (27)$$

where $A = e^{m\alpha - 1 + m\beta C}$. From this expression we derive the average kinetic energy per particle

$$\frac{\int f \frac{1}{2} m v^2 d^3\vec{v}}{\int f d^3\vec{v}} = \frac{\int e^{-m\beta(\frac{1}{2}v^2)} \frac{1}{2} m v^2 d^3\vec{v}}{\int e^{-m\beta(\frac{1}{2}v^2)} d^3\vec{v}} = \frac{3}{2\beta},$$

and therefore we see that β should be interpreted as the inverse temperature

$$\beta = \frac{1}{kT}. \quad (28)$$

Finally, inserting the calculated $f(r, v)$ from (27) into equation (17) we obtain

$$\rho + (1+w)\rho_X = \left(\frac{2\pi kT}{m} \right)^{\frac{3}{2}} m A e^{-\frac{m}{kT}\phi(r)},$$

which for

$$mA = \left(\frac{m}{2\pi kT} \right)^{\frac{3}{2}} [\rho_0 + (1+w)\rho_X] e^{\frac{m}{kT}\phi(0)}$$

leads to equation (14)

$$\rho(r) = [\rho_0 + (1+w)\rho_X] e^{-\frac{m}{kT}[\phi(r) - \phi(0)]} - (1+w)\rho_X \quad (29)$$

and to the distribution (11)

$$f(r, v) = \left(\frac{m}{2\pi kT} \right)^{\frac{3}{2}} \frac{\rho_{\text{eff}}(r)}{m} e^{-\frac{m}{kT}v^2/2},$$

as desired.

In summary, we see that the hydrostatic equilibrium of a self-gravitating gas, in the presence of dark energy, for an isothermal distribution corresponds to a state of entropy extremum, with an effective density given by (13) that obeys the Boltzmann distribution. However, the stability of this state depends on whether the extremum is maximum or not.

C. Energy, temperature and stability

In order to determine the type of the entropy extremum, and thus to deduce whether we have stability or not, we have to examine the sign of the second variation of entropy. Fortunately, due to a theorem of Poincaré [49], and its subsequent refinements by Katz [24, 50], one does not always have to calculate the second variation of entropy or free energy. In particular, for fixed energy E and mass M , that is in the case of microcanonical ensemble, an instability sets in at the equilibrium point where there is a vertical tangent on the diagram of equilibria $T(E)$. On the other hand, for fixed temperature T and mass M , that is in the case of canonical ensemble, an instability sets in at the equilibrium point where there is a vertical tangent on the diagram of equilibria $E(T)$. For an isothermal sphere of a self-gravitating gas, the instability in the microcanonical ensemble is called gravothermal catastrophe [17–19, 35, 36], while the instability in the canonical ensemble is called isothermal collapse [21, 36, 37].

In practice, in a series-of-equilibria diagram of the energy versus any variable, an extremum is a turning point of stability. This implies that if one branch of the diagram up to the turning point is known to be stable, the branch beyond the turning point will be unstable, and vice versa. In addition, since we have an extremum, there do not exist equilibria at all above this extremum in the case where it is a global maximum, or beneath this extremum in the case where it is a global minimum. Therefore, we conclude that the system exhibits a gravothermal catastrophe at the turning point in a series-of-equilibria diagram of E versus any variable, and similarly it exhibits an isothermal collapse at the turning point in a series-of-equilibria diagram of T versus any variable.

In conclusion, instead of having to perform the complicated calculation of the second variation of entropy, we just need to calculate the energy and temperature of the isothermal sphere in the presence of dark energy, and draw the corresponding diagrams of series of equilibria.

Substituting the density distribution (29) into the Poisson equation (15), we obtain the Emden equation [48], modified with the additional contribution of the dark-energy component, namely

$$\frac{1}{r^2} \frac{d}{dr} \left(r^2 \frac{d\phi}{dr} \right) = 4\pi G [\rho_0 + (1+w)\rho_X] e^{-\frac{m}{kT}[\phi(r) - \phi(0)]} + 8\pi G w \rho_X, \quad (30)$$

where ρ_0 is the density of matter at the center of the sphere. Defining the dimensionless variables

$$x = r \sqrt{4\pi G \rho_0 \frac{m}{kT}}, \quad y = \frac{m}{kT} [\phi - \phi(0)], \quad \lambda = \frac{2\rho_X}{\rho_0}, \quad (31)$$

the modified Emden equation (30) becomes:

$$\frac{1}{x^2} \frac{d}{dx} \left(x^2 \frac{dy}{dx} \right) = \left(1 + \frac{1+w}{2} \lambda \right) e^{-y} + w\lambda, \quad (32)$$

with initial conditions $y(0) = y'(0) = 0$. Hence, for given values of w and ρ_X , an equilibrium configuration is completely determined by the values of mass M and radius R that correspond to a temperature T and energy E . In the following we desire to numerically generate a series of equilibria $T(E)$ for fixed mass M in order to study stability, which is not straightforward since there are some complications.

Let z be the value of x at R :

$$z = R\sqrt{4\pi G\rho_0\frac{m}{kT}}. \quad (33)$$

To obtain a solution of equation (32) one has to specify the couple (z, λ) . As we noted, we do not want just a solution, but a consistent series of solutions (equilibria). Assuming some fixed value of ρ_X , then fixing λ and solving for various z would generate a series with different mass at each equilibrium. The reason is that fixing λ corresponds to fixing ρ_0 . Therefore, in order to have different equilibria for various radii R and hence z , these equilibria should have different mass. The same holds if one keeps z constant and vary λ . The deeper reason for this difficulty in determining a consistent series of equilibria, that does not exist without dark energy, is that dark energy introduces a mass scale

$$M_X = \frac{4}{3}\pi R^3 \rho_X \quad (34)$$

to the system. Thus, we introduce a dimensionless mass:

$$\mu = \frac{M}{2M_X} = \frac{\langle \rho \rangle}{2\rho_X}. \quad (35)$$

Based on earlier works [27, 35, 36] we construct a computer code that can solve equation (32) for various values (z, λ) and choose these solutions that correspond to a fixed (up to some tolerance determined by the user) value of μ . In this way, we can generate consistent series of equilibria corresponding to the same mass. Performing the calculation for various μ we can generate the series for various values of ρ_X .

In order to proceed to this numerical elaboration, we define a dimensionless energy

$$\mathcal{E} = \frac{ER}{GM^2}, \quad (36)$$

and a dimensionless inverse temperature

$$\mathcal{B} = \frac{GMm}{RkT}. \quad (37)$$

In order to calculate \mathcal{B} we integrate equation (15), using also the dimensionless variables (31), obtaining

$$\mathcal{B} = zy' - \frac{1}{6}(1 + 3w)\lambda z^2. \quad (38)$$

The calculation of \mathcal{E} is more complicated. We start by using the distribution function (11) in order to calculate

kinetic energy $K \equiv \frac{1}{2}m \int f(r, v)v^2 d^6\tau$, which using the dimensionless variables (31) leads finally to the dimensionless kinetic energy

$$\mathcal{K} \equiv \frac{KR}{GM^2} = \frac{3}{2\mathcal{B}} \left[1 + \frac{1}{6}(1+w)\frac{\lambda z^2}{\mathcal{B}} \right]. \quad (39)$$

Similarly, using (22) we define a dimensionless expression for $\phi(0)$:

$$\frac{m}{kT}\phi(0) = - \left[\left(1 + \frac{1+w}{2}\lambda \right) \int_0^z x e^{-y} dx \right] + \frac{1+w}{4}\lambda z^2, \quad (40)$$

and then inserting (40) into (20),(21),(23), we calculate the dimensionless potential energy as

$$\begin{aligned} \mathcal{U} \equiv \frac{UR}{GM^2} &= \frac{1}{2\mathcal{B}^2 z} \left(1 + \frac{1+w}{2}\lambda \right) \int_0^z x^2 y e^{-y} dx \\ &\quad - \frac{1}{2\mathcal{B}} \left[1 + \frac{1}{6\mathcal{B}}(1+w)\lambda z^2 \right] \\ &\quad \times \left(1 + \frac{1+w}{2}\lambda \right) \int_0^z x e^{-y} dx \\ &\quad + \frac{1}{12\mathcal{B}^2 z} w\lambda \left(1 + \frac{1+w}{2}\lambda \right) \int_0^z x^4 e^{-y} dx. \end{aligned} \quad (41)$$

Finally, using (39) and (41), the dimensionless energy is written as

$$\mathcal{E} = \mathcal{K} + \mathcal{U}. \quad (42)$$

Our scope is to draw the critical radius, at which an instability sets in, in the microcanonical and canonical ensembles, with respect to ρ_X for different w values. To this end, we generate series of equilibria solving (32) with our code (that keeps μ constant) for different μ values that correspond to different ρ_X . In Figure 1 we see the series of equilibria expressed by \mathcal{E} w.r.t. the density contrast ρ_0/ρ_R for each isothermal sphere, for a specific μ , for a simple cosmological constant $w = -1$, quintessential $w = -0.8$ and phantom $w = -1.2$ dark energy. Each minimum is a turning point of stability in the microcanonical ensemble. On the other hand, the maximum in \mathcal{B} is a turning point of stability in the canonical ensemble. We repeat the calculations of minima in \mathcal{E} and maxima in \mathcal{B} for many μ values and finally plot these critical values in Figure 2 and Figure 3. These critical values correspond to the desired critical radii, assuming M, E constant in the microcanonical ensemble and M, T constant in the canonical ensemble.

In Figure 2, for every w we observe the characteristic reentrant behavior for the microrcanonical ensemble noticed firstly in [35]. For a fixed ρ_X , equilibria do exist for arbitrarily small radii. Then, at some bigger radius an instability sets in and no equilibria are allowed. The system undergoes gravothermal catastrophe [17, 18]. Note that recently, gravothermal catastrophe has been identified as similar to Jeans instability [51]. Returning to

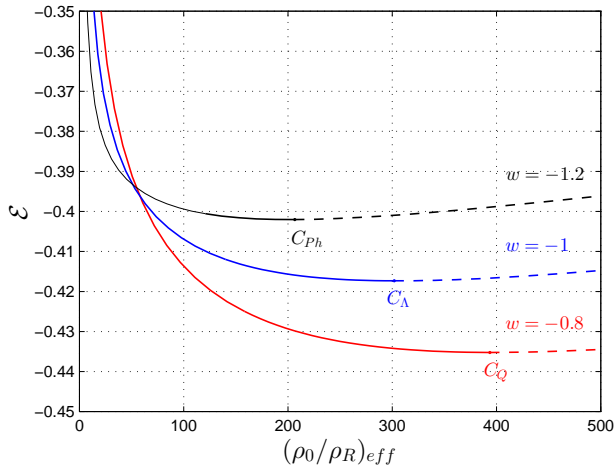


FIG. 1: The series of equilibria expressed as $\mathcal{E} = ER/GM^2$ versus the density contrast $(\rho_0/\rho_R)_{eff}$ for a simple cosmological constant ($w = -1$), quintessential ($w = -0.8$) and phantom ($w = -1.2$) dark energy. At points C_{Ph} , C_{Λ} and C_Q an instability sets in. The dashed curves correspond to unstable equilibria, while the solid curves to stable equilibria.

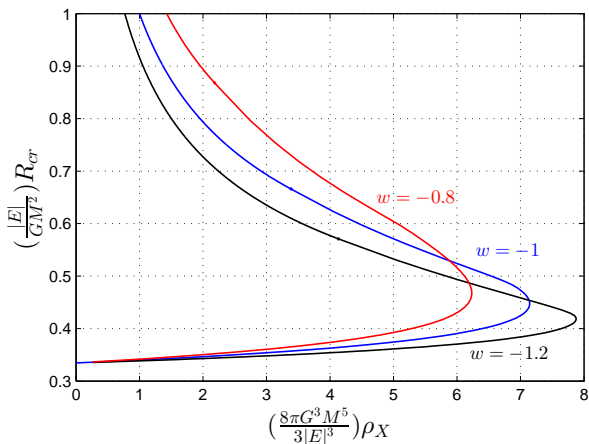


FIG. 2: The critical radius for fixed negative energy E and mass M (microcanonical ensemble) versus ρ_X for cosmological constant ($w = -1$), quintessential ($w = -0.8$) and phantom ($w = -1.2$) dark energy. For each curve, the instability domain is inside it, that is no equilibria exist between the two critical radii for some fixed ρ_X .

Figure 2, we see that for some even bigger radius, let call it the “reentrant radius”, the equilibria are restored. This effect is due to the dark energy, which introduces an harmonic, repulsive force proportional to the radius. The equilibria above this radius have peculiar density profiles, with an increasing density towards the edge or with various local maxima [35, 36]. This means that if the walls were absent, these states would correspond

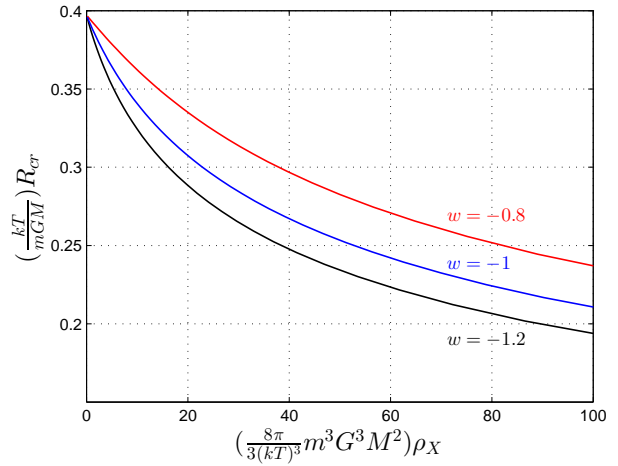


FIG. 3: The critical radius for fixed temperature T and mass M (canonical ensemble) versus ρ_X for cosmological constant ($w = -1$), quintessential ($w = -0.8$) and phantom ($w = -1.2$) dark energy. For each curve the instability domain is the one below the curve, and thus no equilibria exist for radii smaller than the critical radius for some fixed ρ_X .

to perturbations that would follow Universe’s expansion. Such perturbations would not collapse and could not lead to structure formation. Thus, *the reentrant radius, defines the maximum size of a perturbation that can lead to structure formation.* This resembles exactly the “maximum turnaround radius” noticed recently [52]. We see in Figure 2 that the reentrant radius is smaller for phantom dark energy than for quintessential one. Thus, large scale structures are more easily formed in a quintessential rather than a phantom universe. This effect is due to the stronger repulsive pressure of phantom dark energy and it was qualitatively expected, however in the above analysis it has been incorporated quantitatively.

In Figure 3 we notice that the critical radius in the canonical ensemble, is smaller for phantom rather than quintessential dark energy. Since the instability domain is underneath the critical radius, we conclude again that quintessence increases the instability domain, with respect to phantom dark energy and the simple cosmological constant case. In the case of the canonical ensemble, this effect is only due to the effective particles that introduce additional mutual attraction for quintessential dark energy. The negative pressure is not important, because the instability sets in for small radii where the repulsive force is irrelevant (it increases with distance).

Finally, we stress that the minimum in \mathcal{E} corresponds to some value of the density contrast $(\rho_0/\rho_R)_{eff}$, as can be seen in Figure 1. This is a critical value, where an instability sets in. For larger density contrasts, the equilibria are unstable and the system undergoes gravothermal catastrophe. These unstable equilibria correspond to the dashed curves in Figure 1.

In the next section we will use this critical density

contrast, which for completeness is depicted in Figure 4, where we see that the critical density contrast is smaller for phantom rather than quintessential dark energy. Equilibria corresponding to density contrast value that lies above each curve are unstable, while the ones underneath each curve are stable.

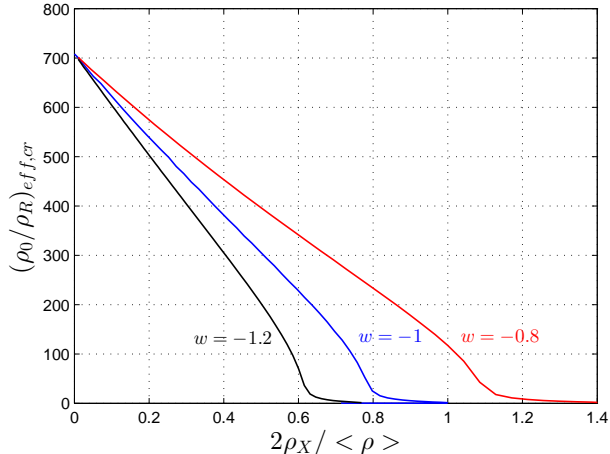


FIG. 4: The critical density contrast of effective density for fixed radius R and mass M versus ρ_X for cosmological constant ($w = -1$), quintessential ($w = -0.8$) and phantom ($w = -1.2$) dark energy in the microcanonical ensemble. For each curve, all equilibria above it are unstable, that is the ones with density contrast bigger than the critical value for some fixed ρ_X .

III. GALAXY CLUSTERS IN THE PRESENCE OF DARK ENERGY

In the previous section we performed a detailed general analysis of the stability of self-gravitating gas in the presence of a general dark-energy component. In this section we will apply it in the specific case of galaxy clusters, which are dominated by the dark matter halo. Our goal is to first estimate the effect of dark energy on the density profile of the dark-matter halo and secondly to examine whether any constrain on the equation-of-state of dark energy can be deduced from observational facts of galaxy clusters. We will perform the analysis in the most simple set-up, assuming hydrostatic equilibrium, isothermal distribution and spherical symmetry.

Galaxy clusters are the largest, virialized, self-gravitating bound systems in the Universe. They have been the focus of intense study for several decades, among other reasons because they provide crucial information on the formation of large-scale structure and on estimates of cosmological parameters [53]. Galaxy clusters are consisted of three components. Dark matter is the main component holding about 80 – 90% of the total mass, the X-ray emitting hot intracluster medium (ICM)

makes up about 10 – 20% and only a small fraction $\sim 1\%$ corresponds to cold gas, dust and stars found mainly in galaxies. The intracluster medium is hot plasma with temperature about 2 – 10keV, consisted mainly of ionized hydrogen and helium and electrons. It emits X-rays due to thermal bremsstrahlung. All three components are found to be approximately in hydrostatic equilibrium [54, 55] inside the gravitational well of the cluster, dominated by the dark matter halo. The hypothesis of hydrostatic equilibrium corresponds to the assumption that self-gravity is halted only by thermal pressure. Non-thermal pressure is found to contribute at about 10% [56–58] to the total pressure. Dark matter is assumed to be collisionless, although recently the possibility to be slightly self-interacting is being inspected [59–62]. The ICM is nearly isothermal, at least apart from the central regions [63, 64].

Due to the equivalence between inertial and gravitational mass, orbits in a gravitational system are independent of the mass of the orbiting particles. Therefore, it is legitimate to assume that different species in a relaxed, spherically-symmetric, gravitational system have the same average specific kinetic energy. In a gas system, equilibrium implies energy equipartition between different species, while for a relaxed, gravitational system the corresponding principle would be the common velocity dispersion, because of the equivalence principle. Indeed, simulations of dark matter haloes [65, 66] do indicate that $(k\bar{T}/m)/\sigma_{DM}^2 \simeq 1$ while observational data indicate [67] that $(k\bar{T}/m)/\sigma_{gal}^2 \simeq 1$, where \bar{T} is the mean temperature of the ICM, σ_{DM}^2 is the dark matter velocity dispersion, σ_{gal}^2 is the galaxy velocity dispersion, $m \simeq 0.6m_p$ is the mean particle mass of ICM and m_p is the proton mass. Therefore, we have strong arguments to justify the consideration

$$\sigma_{DM}^2 = \sigma_{gal}^2 = \frac{kT}{m}, \quad (43)$$

where T is the temperature of ICM in an isothermal distribution. Consequently, under these assumptions, the three components of a galaxy cluster have the same density distributions, leading to the total distribution:

$$\rho(r) = \rho_0 e^{-\frac{r}{R}} [\phi(r) - \phi(0)]. \quad (44)$$

In realistic situations not all components have the same distributions, but since in this work we are interested in estimating the effect of dark energy to the distribution of the cluster, and not determining the exact distributions, we expect that deviations from expressions (43) and (44) would not alter the dark-energy effect. Since clusters are dominated by the dark matter halo, our results hold for the halo’s profile. Additionally, it is interesting to note that the above assumptions are exactly the same with those of the so-called truncated isothermal sphere (TIS) model [69, 70]. In TIS model the dark-matter halo is assumed to be spherical, isothermal and in equilibrium (that is an isothermal sphere), formed from the collapse

Cluster	z	M_{vir}	R_{vir}	T	$\frac{2\rho_X}{\langle\rho\rangle}$
MS 0906+11	0.1704	8.3	1737	6.1	0.0103
MS 1224+20	0.3255	3.8	1226	4.8	0.0079
MS 1358+62	0.3290	10.3	1706	6.7	0.0079
MS 1512+36	0.3727	3.3	1139	4.1	0.0073
MS 1621+26	0.4275	12.3	1715	8.1	0.0067
A68	0.2550	10.5	1790	8.0	0.0089
A267	0.2300	7.5	1623	5.9	0.0093
A963	0.2060	6.5	1569	6.6	0.0097
A1763	0.2230	13.5	1982	7.7	0.0094
A2218	0.1756	8.8	1766	7.0	0.0102
A2219	0.2256	11.3	1865	9.8	0.0094

TABLE I: The redshift z , virial mass $M_{vir}(10^{14}h^{-1}M_{\odot})$, virial radius $R_{vir}(h^{-1}kpc)$, temperature $T(keV)$ and the ratio of the cosmological constant to the mean density for $\rho_X = 6.5 \cdot 10^{-30} gr/cm^3$ for some galaxy clusters. The virial mass is calculated by Hoekstra [68] with a NFW fit to weak-lensing data.

and virialization of “top-hat” density-perturbations. The TIS scenario is a unique, non-singular solution of the Emden equation, modified with a cosmological constant [70], corresponding to the minimum-energy solution under constant external pressure, while the gas and the dark-matter halo are assumed to have the same distribution as in equation (44). The difference of TIS with our analysis is that we consider all non-singular solutions of the modified Emden equation (32) and not only the specific TIS one. This model is in a very good agreement with simulations and observations [71], at least outside the inner regions of the cluster. In the inner regions the TIS model predicts a soft core, however collisionless N -body simulations of dark matter haloes predict a cusp, rather than a core. The main reason for this difference is the assumption of isothermality: the N -body simulations are nearly isothermal apart from a small region dip near the center, which causes the cuspy profile, while the self-interacting dark matter is possible to form a central core [72]. Moreover, in contrast with simulations, observations at small scales favor the existence of a central core in dark matter haloes, a problem called the “core-cusp problem” [73, 74]. Regarding our work, the agreement of the non-singular, isothermal sphere with observations and simulations, besides the inner region, is sufficient for our purposes.

Let us now proceed to the estimation of the effect of dark energy to the density profile of galaxy clusters. Note that the effective mass and density profile are the ones measured by indirect measurements such as gravitational lensing and hydrostatic equilibrium. Thus, in all of our subsequent analysis of galaxy clusters we use the effective values of density contrast (for the cosmological constant $w = -1$ however the effective density is identical to the matter density).

In the estimation procedure we will need the quantity

$2\rho_X/\langle\rho\rangle$ in galaxy clusters, where $\langle\rho\rangle = 3M_{vir}/4\pi R_{vir}^3$ is the average density of the cluster as it arises from observations. In order to extract this observation-related value, we work with a sample of 11 clusters taken by Hoekstra [68], who performed a model-independent analysis based on weak-lensing measurements. We used only these clusters that have such virial radius, virial mass and temperature that can correspond to an isothermal equilibrium. The virial radius, the virial mass, the temperature and the ratio $2\rho_X/\langle\rho\rangle$ for each cluster is shown in Table I. We have used $\rho_X \simeq 6.5 \cdot 10^{-30} gr/cm^3$ [1]. The mean ratio $2\rho_X/\langle\rho\rangle$ is:

$$\frac{1}{\mu} = \left\langle \frac{2\rho_X}{\langle\rho\rangle} \right\rangle = 0.009, \quad (45)$$

and the mean $\mathcal{B} = GM_{vir}m/kTR_{vir}$ is

$$\langle\mathcal{B}\rangle = 2.07. \quad (46)$$

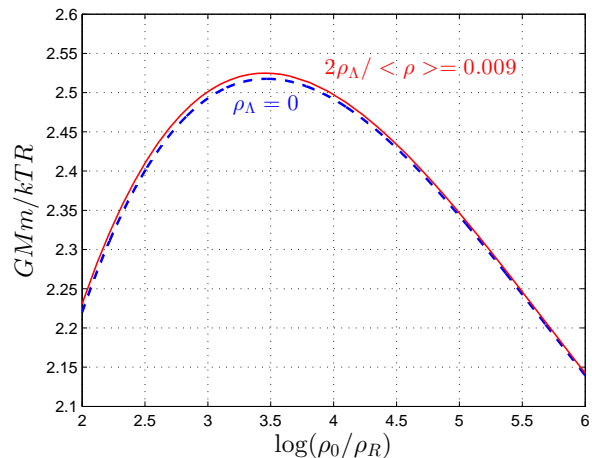


FIG. 5: The series of equilibria without dark energy (dashed blue line) and with a cosmological constant, i.e. $w = -1$, (solid red line) for $2\rho_X/\langle\rho\rangle = 0.009$ that corresponds to our galaxy clusters sample, expressed as the ratio GMm/kTR versus the natural logarithm of the central to edge density ratio of the cluster. At $GMm/kTR = 2.07$ correspond two density profiles at each case ($\rho_\Lambda = 0$ and $\rho_\Lambda \neq 0$). The profiles with the higher density contrast (after the peak) are the ones relevant to galaxy clusters. The case $\rho_\Lambda \neq 0$ has greater density contrast than the case $\rho_\Lambda = 0$.

Using the computer code of the previous section, and for dimensionless mass (equation (35)) $\mu = 111.11$ that corresponds to (45), we calculate numerically the corresponding value to (46) of the effective density contrast $(\rho_0/\rho_R)_{\text{eff}}$ both in the presence of dark energy and for $\rho_X = 0$ and find how much is the profile altered by the presence of dark energy. For fixed radius, mass and temperature, we find the counter-intuitive result that dark energy, either quintessential or phantom or a cosmological constant, tends to steepen the density profile increasing the density contrast. This can be seen in figure 5 for

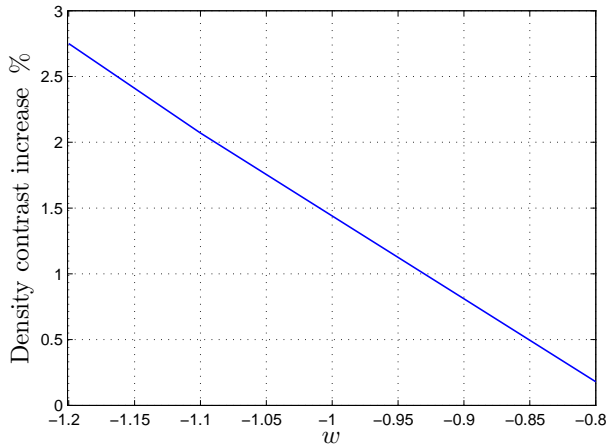


FIG. 6: The effect of dark energy to the density profile of galaxy clusters. The percentage increase of the effective density contrast $(\rho_0/\rho_R)_{\text{eff}}$, i.e. the center divided by the edge density, for $\rho_X = 6.5 \cdot 10^{-30} \text{ gr/cm}^3$ with respect to the case $\rho_X = 0$ versus w , for fixed temperature, total mass and radius.

density contrast values greater than the peak, which are the ones relevant to observations. We believe the reason is that for fixed temperature, mass and radius, the extra outward pressure introduced by dark energy, enables more mass to be concentrated towards the center of the cluster. For the case $w = -1$, i.e. the cosmological constant, we find that the density profile is steepened by an amount of 1.5%. Finally, we mention that the effect of dark energy becomes stronger as w becomes more negative, as can be seen in figure 6.

Finally, let us propose a method to impose constraints on the dark-energy equation-of-state parameter. As we discussed in section II, as w attains more negative values, the critical density contrast (the maximum allowed before gravothermal catastrophe occurs) decreases, as in figure 4. Therefore, we can use this property in order to find a minimum allowed value of w . If the minimum possible density contrast, corresponding to an isothermal distribution can be determined from clusters' observations, then the critical density contrast can be no smaller than this value. Hence, provided the minimum observational density contrast is given, we can numerically calculate the w which has critical density contrast equal to this value. This w value would be the minimum possible in order for the cluster to be in equilibrium.

IV. CONCLUSIONS

In this work we studied the effect of dark energy on the stability of isothermal spheres for various values of ρ_X (in section II), and furthermore, based on this analysis, we focused on the effect of dark energy on galaxy clusters

(in section III).

We assumed a linear equation of state for dark energy and we investigated the effect on self-gravitating gas bound by external pressure (walls), in the Newtonian limit. Dark energy introduces a repulsive force due to the negative pressure, generated by an effective potential (equation (21)), but it additionally introduces “dark energy” particles through an effective density, given in equation (9). These dark energy particles strengthen attraction in case of quintessential dark energy ($w > -1$) and weaken attraction in case of phantom dark energy ($w < -1$). The total effect, however, of repulsive potential and dark energy particles, is in all cases repulsive. We calculated the entropy extremum and we found that it corresponds to a Boltzmann distribution for the effective density (see equations (13) and (29)).

Then, we focused on the effect of dark energy in the stability of isothermal spheres. This effect can be summarized in figures 2, 3 and 4. The microcanonical ensemble (fixed energy) in the presence of a cosmological constant is known to present a reentrant phase transition [35], that is for some fixed ρ_X there exist two critical radii and no equilibria exist between these two values. The upper radius is called the reentrant radius and at this radius equilibria are restored. This equilibria have increasing density towards the edge and correspond to perturbations that follow the expansion in an expanding Universe. Thus, *the reentrant radius, defines the maximum size of a perturbation that can lead to structure formation*. Quintessence increases the reentrant radius, while phantom dark energy decreases it, as can be seen in Figure 2. Therefore, a quintessence universe is expected to present richer large scale structure, with more and larger bounded systems, than a phantom universe. In the canonical ensemble (fixed temperature) there is only one critical radius less than which there are no equilibria. Quintessence increases this critical radius with respect to the simple cosmological constant case, while phantom dark energy decreases it, as can be seen in Figure 3. Thus, quintessential dark energy enlarges the instability domain, while phantom dark energy narrows it, with respect to the cosmological constant. Finally, we inspected how the critical effective density contrast (the critical central to edge effective density ratio), corresponding to gravothermal catastrophe (fixed energy) is affected by dark energy. The result is shown in Figure 4. Quintessential dark energy increases the critical density contrast, while phantom dark energy decreases it. This implies that in a quintessence universe more condensed large scale structures are formed.

Regarding the second part of this work (section III), let us remark that we find a rather counter-intuitive result. Dark energy causes the density profile of galaxy clusters to be more centrally concentrated. That is, for fixed mass, radius and temperature, the system will equilibrate in a larger density contrast (central to edge ratio ρ_0/ρ_R) in the presence of dark energy. This is manifested in Figure 5. It seems as if for these equilibria, the extra

outward pointing pressure of dark energy is added to the thermal pressure, enabling the system to equilibrate in a more condensed state. This might be associated with the fact that these equilibria are unstable under variations that preserve the temperature, namely isothermal collapse. This is evident in Figure 5, where the equilibria corresponding to galaxy clusters are the ones after the peak and hence are unstable under isothermal collapse. However, they are stable under variations that preserve the energy (instability in this case would correspond to gravothermal catastrophe), at least up to some greater density contrast value. Most importantly, this effect, that is the steepening of the density profile due to dark energy, corresponds in the case $w = -1$ to equilibration of the cluster for the same M , T and R at about 1.5% greater density contrast. The effect is getting stronger as w attains more negative values. This is evident in Figure 6.

Last but not least, we proposed a method to constrain phantom dark energy from galaxy clusters observations. As we have seen in section II the critical density contrast at which the instability sets in is decreasing with decreasing w . Therefore, if one can determine, based on galaxy clusters observations, the density contrast corresponding to static isothermal equilibrium, then one can determine the minimum w as the one that has critical density contrast equal to this value.

Acknowledgments

The research of ENS is implemented within the framework of the Action ‘‘Supporting Postdoctoral Researchers’’ of the Operational Program ‘‘Education and Lifelong Learning’’ (Actions Beneficiary: General Secretariat for Research and Technology), and is co-financed by the European Social Fund (ESF) and the Greek State.

Appendix A

We derive the TOV equations (6) and (7). Any spherically symmetric metric can be written in the form:

$$ds^2 = e^\nu c^2 dt^2 - e^\lambda dr^2 - d\Omega,$$

where in general $\nu = \nu(r, t)$ and $\lambda = \lambda(r, t)$. The Einstein’s equations

$$R^\mu_\nu - \frac{1}{2}R\delta^\mu_\nu = \frac{8\pi G}{c^4}T^\mu_\nu$$

give:

$$\frac{8\pi G}{c^4}T^0_0 = e^{-\lambda} \left(\frac{\lambda'}{r} - \frac{1}{r^2} \right) + \frac{1}{r^2} \quad (\text{A1})$$

$$\frac{8\pi G}{c^4}T^1_1 = -e^{-\lambda} \left(\frac{\nu'}{r} + \frac{1}{r^2} \right) + \frac{1}{r^2} \quad (\text{A2})$$

$$\begin{aligned} \frac{8\pi G}{c^4}T^2_2 = \frac{8\pi G}{c^4}T^3_3 = & -e^{-\lambda} \left(\frac{\nu''}{2} - \frac{\lambda'\nu'}{4} + \frac{\nu'^2}{4} + \frac{\nu' - \lambda'}{2r} \right) \\ & + e^{-\nu} \left(\frac{\ddot{\lambda}}{2} + \frac{\dot{\lambda}^2}{4} - \frac{\dot{\lambda}\dot{\nu}}{4} \right) \end{aligned} \quad (\text{A3})$$

$$\frac{8\pi G}{c^4}T^1_0 = -e^{-\lambda} \frac{\dot{\lambda}}{r} \quad (\text{A4})$$

$$\frac{8\pi G}{c^4}T^0_1 = e^{-\nu} \frac{\dot{\lambda}}{r}, \quad (\text{A5})$$

where a prime denote differentiation w.r.t. r and a dot w.r.t. t . We set the energy momentum tensor to be that of a perfect fluid in the presence of ρ_X with $p_X = w\rho_X c^2$, that is

$$T^\mu_\nu = (\tilde{p} + \tilde{\rho}c^2)g_{\alpha\nu} \frac{dx^\mu}{ds} \frac{dx^\alpha}{ds} - \tilde{p}\delta^\mu_\nu, \quad (\text{A6})$$

with $\tilde{\rho} = \rho + \rho_X$ and $\tilde{p} = p + w\rho_X c^2$. At the equilibrium it is just $T^\mu_\nu \rightarrow (\tilde{\rho}c^2, -\tilde{p}, -\tilde{p}, -\tilde{p})$ and $\dot{\lambda} = 0$, $\dot{\nu} = 0$. Substituting into Einstein’s equations and after some calculations, equations (A1-A5) give:

$$\frac{dp}{dr} = -\frac{1}{2}(p + \rho c^2 + (1+w)\rho_X c^2)\nu' \quad (\text{A7})$$

$$\frac{8\pi G}{c^2}\rho = e^{-\lambda} \left(\frac{\lambda'}{r} - \frac{1}{r^2} \right) + \frac{1}{r^2} - \frac{8\pi G}{c^2}\rho_X \quad (\text{A8})$$

$$\frac{8\pi G}{c^4}p = e^{-\lambda} \left(\frac{\nu'}{r} + \frac{1}{r^2} \right) - \frac{1}{r^2} - w\frac{8\pi G}{c^2}\rho_X, \quad (\text{A9})$$

which by the transformation

$$e^{-\lambda} = 1 - \frac{2GM(r)}{rc^2} - \frac{8\pi G}{3c^2}\rho_X r^2 \quad (\text{A10})$$

become just two equations, namely

$$\frac{dp}{dr} = - \left[\frac{p}{c^2} + \rho + (1+w)\rho_X \right] \left[\frac{GM(r)}{r^2} + 4\pi G \frac{p}{c^2} r + \frac{4\pi G}{3} \rho_X r(1+3w) \right] \left(1 - \frac{2GM(r)}{rc^2} - \frac{8\pi G}{3c^2} \rho_X r^2 \right)^{-1} \quad (\text{A11})$$

$$\frac{dM(r)}{dr} = 4\pi\rho r^2. \quad (\text{A12})$$

-
- [1] WMAP, G. Hinshaw *et al.*, *ApJSuppl.* **208**, 19 (2013), arXiv:1212.5226.
- [2] R. Amanullah *et al.*, *Astrophys.J.* **716**, 712 (2010), arXiv:1004.1711.
- [3] C. Blake *et al.*, *Mon.Not.Roy.Astron.Soc.* **418**, 1707 (2011), arXiv:1108.2635.
- [4] B. Ratra and P. Peebles, *Phys.Rev.* **D37**, 3406 (1988).
- [5] C. Wetterich, *Nucl.Phys.* **B302**, 668 (1988).
- [6] A. R. Liddle and R. J. Scherrer, *Phys.Rev.* **D59**, 023509 (1999), astro-ph/9809272.
- [7] S. Basilakos and M. Plionis, *ApJ* **593**, L61 (2003), astro-ph/0306105.
- [8] Z.-K. Guo, N. Ohta, and Y.-Z. Zhang, *Mod.Phys.Lett.* **A22**, 883 (2007), astro-ph/0603109.
- [9] S. Dutta and R. J. Scherrer, *Phys.Rev.* **D78**, 123525 (2008), arXiv:0809.4441.
- [10] S. Dutta, E. N. Saridakis, and R. J. Scherrer, *Phys.Rev.* **D79**, 103005 (2009), arXiv:0903.3412.
- [11] R. Caldwell, *Phys.Lett.* **B545**, 23 (2002), astro-ph/9908168.
- [12] R. R. Caldwell, M. Kamionkowski, and N. N. Weinberg, *Phys.Rev.Lett.* **91**, 071301 (2003), astro-ph/0302506.
- [13] S. Nojiri and S. D. Odintsov, *Phys.Lett.* **B562**, 147 (2003), hep-th/0303117.
- [14] V. Onemli and R. Woodard, *Phys.Rev.* **D70**, 107301 (2004), gr-qc/0406098.
- [15] E. N. Saridakis, *Phys.Lett.* **B676**, 7 (2009), arXiv:0811.1333.
- [16] X.-m. Chen, Y.-g. Gong, and E. N. Saridakis, *JCAP* **0904**, 001 (2009), arXiv:0812.1117.
- [17] V. Antonov, *Vest. Leningrad Univ.* **7**, 135 (1962).
- [18] D. Lynden-Bell and R. Wood, *MNRAS* **138**, 495 (1968).
- [19] T. Padmanabhan, *ApJS* **71**, 651 (1989).
- [20] T. Padmanabhan, *Phys. Rep.* **188**, 285 (1990).
- [21] P.-H. Chavanis, *A&A* **381**, 340 (2001), astro-ph/0103159.
- [22] H. de Vega and N. Sanchez, *Nucl.Phys.* **B625**, 409 (2002), astro-ph/0101568.
- [23] H. de Vega and N. Sanchez, *Nucl.Phys.* **B625**, 460 (2002), astro-ph/0101567.
- [24] T. Katz, *Found. Phys.* **33**, 223 (2003).
- [25] R. Sorkin, R. Wald, and Z. Z.J., *Gen. Rel. Grav.* **13**, 1127 (1981).
- [26] S. Gao, *Phys.Rev.* **D84**, 104023 (2011), arXiv:1109.2804.
- [27] Z. Roupas, *Class.Quant.Grav.* **30**, 115018 (2013), arXiv:1301.3686.
- [28] Z. Roupas, *Proceedings:Barcelona Postgrad encounters on fundamental physics, Universitat de Barcelona*, 31 (2013), arXiv:1305.4851.
- [29] C. Anastopoulos and N. Savvidou, (2013), arXiv:1302.4407.
- [30] S. R. Green, J. S. Schiffrin, and R. M. Wald, (2013), arXiv:1309.0177.
- [31] J. S. Schiffrin and R. M. Wald, (2013), arXiv:1310.5117.
- [32] X. Fang and S. Gao, (2013), arXiv:1311.6899.
- [33] H. de Vega and J. Siebert, *Nucl.Phys.* **B707**, 529 (2005), astro-ph/0305322.
- [34] H. de Vega and J. Siebert, *Nucl.Phys.* **B726**, 464 (2005), astro-ph/0410147.
- [35] M. Axenides, G. Georgiou, and Z. Roupas, *Phys.Rev.* **D86**, 104005 (2012), arXiv:1206.2839.
- [36] M. Axenides, G. Georgiou, and Z. Roupas, *Nucl. Phys.* **B871**, 21 (2013), arXiv:1302.1977.
- [37] M. Axenides, G. Georgiou, and Z. Roupas, *J.Phys.Conf.Ser.* **410**, 012130 (2013), arXiv:1303.4543.
- [38] D. Mota and C. van de Bruck, *Astron.Astrophys.* **421**, 71 (2004), astro-ph/0401504.
- [39] S. Basilakos, J. Bueno Sanchez, and L. Perivolaropoulos, *Phys.Rev.* **D80**, 043530 (2009), arXiv:0908.1333.
- [40] I. L. Shapiro and J. Sola, *JHEP* **0202**, 006 (2002), hep-th/0012227.
- [41] A. Polyakov, *Nucl.Phys.* **B834**, 316 (2010), arXiv:0912.5503.
- [42] S. Basilakos, J. A. S. Lima, and J. Sola, *Int.J.Mod.Phys.* **D** (2013), arXiv:1307.6251.
- [43] C. Wetterich, *Astron.Astrophys.* **301**, 321 (1995), hep-th/9408025.
- [44] A. P. Billyard and A. A. Coley, *Phys.Rev.* **D61**, 083503 (2000), astro-ph/9908224.
- [45] C. G. Boehmer, G. Caldera-Cabral, R. Lazkoz, and R. Maartens, *Phys.Rev.* **D78**, 023505 (2008), 0801.1565.
- [46] R. Tolman, *Phys. Rev.* **55**, 364 (1939).
- [47] J. Oppenheimer and G. Volkoff, *Phys. Rev.* **55**, 374 (1939).
- [48] J. Binney and S. Tremaine, *Galactic Dynamics* (Princeton, 1987).
- [49] H. Poincaré, *Acta. Math.* **7**, 259 (1885).
- [50] T. Katz, *MNRAS* **183**, 765 (1978).
- [51] M. Sormani and G. Bertin, (2013), arXiv:1301.6038.
- [52] V. Pavlidou and T. N. Tomaras, (2013), arXiv:1310.1920.
- [53] S. W. Allen, A. E. Evrard, and A. B. Mantz, *Ann.Rev.Astron.Astrophys.* **49**, 409 (2011), arXiv:1103.4829.
- [54] C. L. Sarazin, *Reviews of Modern Physics* **58**, 1 (1986).
- [55] A. Kravtsov and S. Borgani, *Ann.Rev.Astron.Astrophys.* **50**, 353 (2012), arXiv:1205.5556.
- [56] A. Faltenbacher, A. V. Kravtsov, D. Nagai, and S. Gotzlober, *MNRAS* **358**, 139 (2005), astro-ph/0408488.
- [57] P. Schuecker, A. Finoguenov, F. Miniati, H. Bohringer, and U. Briel, *Astron.Astrophys.* **426**, 387 (2004), astro-ph/0404132.
- [58] E. Rasia *et al.*, *MNRAS* **369**, 2013 (2006), astro-ph/0602434.
- [59] D. N. Spergel and P. J. Steinhardt, *Phys.Rev.Lett.* **84**, 3760 (2000), astro-ph/9909386.
- [60] S. W. Randall, M. Markevitch, D. Clowe, A. H. Gonzalez, and M. Bradac, *ApJ* **679**, 1173 (2008), arXiv:0704.0261.
- [61] M. Bradac *et al.*, *ApJ* **687**, 956 (2008), arXiv:0806.2320.
- [62] M. H. Chan, *MNRAS* **433**, 2310 (2013), arXiv:1305.4465.
- [63] T. H. Reiprich and H. Bohringer, *ApJ* **567**, 716 (2002), astro-ph/0111285.
- [64] S. LaRoque *et al.*, *ApJ* **652**, 917 (2006), astro-ph/0604039.
- [65] O. Host *et al.*, *ApJ* **690**, 358 (2009), arXiv:0808.2049.
- [66] A. E. Evrard *et al.*, *ApJ* **672**, 122 (2008), astro-ph/0702241.
- [67] Y.-J. Xue and X.-P. Wu, *ApJ* **538**, 65 (2000), astro-ph/0002446.
- [68] H. Hoekstra, *MNRAS* **379**, 317 (2007), arXiv:0705.0358.
- [69] P. R. Shapiro and I. T. Iliev, *MNRAS* **307**, 203 (1999), astro-ph/9810164.
- [70] I. T. Iliev and P. R. Shapiro, *MNRAS* **325**, 468 (2001),

- astro-ph/0101067.
- [71] P. R. Shapiro, I. T. Iliev, H. Martel, K. Ahn, and M. A. Alvarez, (2004), astro-ph/0409173.
- [72] K.-J. Ahn and P. R. Shapiro, MNRAS **363**, 1092 (2005), astro-ph/0412169.
- [73] L. Hui, Phys.Rev.Lett. **86**, 3467 (2001), astro-ph/0102349.
- [74] W. de Blok, Adv.Astron. **2010**, 789293 (2010), arXiv:0910.3538.